Journal of Solid State Chemistry 181 (2008) 3145–3150

Contents lists available at ScienceDirect

Journal of Solid State Chemistry

journal homepage: www.elsevier.com/locate/jssc

Thermoelectric properties of polycrystalline $La_{1-x}Sr_xCoO_3$

Kouta Iwasaki [a,*], Tsuyoshi Ito [a], Takanori Nagasaki [b], Yuji Arita [b], Masahito Yoshino [a], Tsuneo Matsui [a,b]

[a] Department of Materials, Physics and Energy Engineering, Graduate School of Engineering, Nagoya University, Furo-cho, Chikusa-ku, Nagoya 464-8603, Japan
[b] EcoTopia Science Institute, Nagoya University, Furo-cho, Chikusa-ku, Nagoya 464-8603, Japan

ARTICLE INFO

Article history:
Received 2 April 2008
Received in revised form
30 July 2008
Accepted 12 August 2008
Available online 22 August 2008

Keywords:
Thermoelectric
Power factor
$LaCoO_3$
Perovskite
Thermopower

ABSTRACT

Thermoelectric properties of polycrystalline $La_{1-x}Sr_xCoO_3$, where Sr^{2+} is substituted in La^{3+} site in perovskite-type $LaCoO_3$, have been investigated. Sr-doping increases the electrical conductivity (σ) of $La_{1-x}Sr_xCoO_3$, and also decreases the Seebeck coefficient (S) for $0.01 \leqslant x \leqslant 0.40$. A Hall coefficient measurement reveals that the increase in electrical conductivity arises from increases in both carrier concentration and the Hall mobility. The decrease in the Seebeck coefficient is caused by a decrease in carrier effective mass as well as increase in carrier concentration. The highest power factor (σS^2) is $3.7 \times 10^{-4}\,W\,m^{-1}\,K^{-2}$ at 250 K for $x = 0.10$. The thermal conductivity (κ) is about $2\,W\,m^{-1}\,K^{-1}$ at 300 K for $0 \leqslant x \leqslant 0.04$, and increases for $x \geqslant 0.05$ because of an increase in heat transport by conductive carrier. The thermoelectric properties of $La_{1-x}Sr_xCoO_3$ are improved by Sr-doping, and the figure of merit ($Z = \sigma S^2 \kappa^{-1}$) reaches $1.6 \times 10^{-4}\,K^{-1}$ for $x = 0.06$ at 300 K ($ZT = 0.048$). For heavily Sr-doped samples, the thermoelectric properties diminish mainly because of the decrease in the Seebeck coefficient and the increase in thermal conductivity.

1. Introduction

Recycling of waste heat is important for efficient use of energy. Thermoelectric materials are viable candidates for waste heat recycling since they can directly convert heat into electrical energy. The energy conversion performance of thermoelectric materials is evaluated using the figure of merit (Z), defined as $Z = \sigma S^2 \kappa^{-1}$ (σ is the electrical conductivity, S the Seebeck coefficient, and κ the thermal conductivity). The numerator, σS^2, is related to electric power for thermoelectric generation and is referred to as the power factor.

Oxide ceramics have received attention as thermoelectric materials since they are relatively stable compared to intermetallic compounds in high-temperature oxidizing atmospheres. In perovskite-type oxides, several 3*d* transition-metal oxides have been reported to show high thermoelectric performances, e.g., p-type (La,*M*)CoO_3 [1], n-type (Sr,*M*)TiO_3 [2–4], and (Ca,*M*)MnO_3 [5,6] (*M* shows metals). In $LaCoO_3$, hole doping improves thermoelectric properties [1,7–10], e.g., Androulakis et al. have reported $Z = 6 \times 10^{-4}\,K^{-1}$ at 300 K ($ZT = 0.18$) for polycrystalline $La_{0.95}Sr_{0.05}CoO_3$. Thermoelectric properties of single-crystal (La,Sr)CoO_3 have been also studied below 300 K by Berggold et al. [8], and there have been several studies on thermoelectric properties of polycrystalline $La_{1-x}Sr_xCoO_3$ [7,9] and $La_{0.9}A_{0.1}CoO_3$ (*A* = Pb, Na) [10]. Thermoelectric properties of hole-doped $LaCoO_3$ are of interest. However, the doping level dependencies of electrical properties are not consistent among previous reports: some groups reported a large S of about $700\,\mu V\,K^{-1}$ for $La_{0.95}Sr_{0.05}CoO_3$ at 300 K [1,11], whereas S of other groups was about $250\,\mu V\,K^{-1}$ for samples of the same composition at the same temperature [8,9]. Such a discrepancy points out the need for further investigations on transport properties of $La_{1-x}Sr_xCoO_3$, although the relationship between physical properties and Sr content has been widely studied [12–22].

In the present study, we prepared polycrystalline $La_{1-x}Sr_xCoO_3$, and investigated the Sr-doping level dependence of thermoelectric properties and the effect of Sr-doping on carrier concentration and the Hall mobility for $0 \leqslant x \leqslant 0.40$.

2. Experimental

$La_{1-x}Sr_xCoO_3$ was prepared by a conventional solid-state reaction. La_2O_3 (99.99%, RARE METALLIC), $SrCO_3$ (99.99+%, RARE METALLIC), Co_3O_4 (99.95%, KANTO CHEMICAL) powders were used as starting materials. These powders were mixed in the appropriate proportion (molar ratios of metals were La:Sr:Co = $1-x:x:1$) in an agate mortar with ethanol, and pressed into a pellet form. The pellets were heated at 1273 K for 20 h in air. After heating, the samples were ground, re-pressed into a pellet form, and sintered at 1673 K for 20 h. In each heating–sintering

* Corresponding author. Fax: +81 52 789 3779.
E-mail address: k-iwasaki@nucl.nagoya-u.ac.jp (K. Iwasaki).

0022-4596/$ - see front matter © 2008 Elsevier Inc. All rights reserved.
doi:10.1016/j.jssc.2008.08.017

process, samples were put on other pellets having the same compositions to avoid any reaction with a Pt crucible.

Powder X-ray diffraction (XRD) data were collected with a diffractometer (RIGAKU, RINT2200) using Cu$K\alpha$ radiation with a pyrolytic graphite monochromator. The lattice parameters were refined by the Rietveld method using the program RIETAN-2000 [23] with XRD data in the range $10 \leqslant 2\theta \leqslant 120^\circ$ (scan step 0.03°) at room temperature. Oxygen content in $La_{1-x}Sr_xCoO_{3-\delta}$ was determined by an iodometric titration. Electrical conductivity was measured by the direct-current four-probe method in the temperature range $100 \leqslant T \leqslant 1100$ K in air. Heating and cooling measurements were performed at a rate of 200 K h^{-1} above 300 K. Electrical conductivity of non-doped $LaCoO_3$ was measured by the van der Pauw method below 300 K. The Seebeck coefficient was determined by the least-squares method from a plot of thermal electromotive force (ΔV) vs. temperature difference (ΔT), and the contribution of lead wires (Pt) was subtracted. The Hall coefficient was measured using a commercial apparatus (TOYO, ResiTest8300) under a magnetic field of 0.7 T. In the calculation of carrier concentration, the Hall scattering factor (γ_H) was assumed to be 1. The experimental error of the measured Hall coefficient was about $\pm 20\%$ for each sample. Thermal conductivity was calculated from bulk density, specific heat, and thermal diffusivity measured by a laser flush technique (ULVAC-RIKO, TC-7000).

3. Results and discussion

A single phase of $La_{1-x}Sr_xCoO_3$ was obtained for $0 \leqslant x \leqslant 0.50$. Bulk densities of sintered pellets were 92–97% of the theoretical density. Fig. 1 shows the rhombohedral lattice parameters of $La_{1-x}Sr_xCoO_3$. The a-axis increased with increasing Sr content, and the increase leveled off for heavily Sr-doped samples. Axial angle (α) linearly decreased toward 60°, indicating that the lattice tends to vary from rhombohedral to cubic with increasing Sr content. The decrease in α by Sr-doping is consistent with previous reports [14,15,20,21], although a discontinuous change around $x = 0.125$ reported in Refs. [14,15] is not observed. The unit cell volume was maximum at $x = 0.30$, and decreased with Sr content for $x \geqslant 0.30$.

For $La_{1-x}Sr_xCoO_{3-\delta}$, oxygen content is known to depend on the Sr content and preparation conditions [8,16,24–26]. Fig. 2 shows the oxygen content for the present samples. As shown in the figure, samples were almost stoichiometric for $x \leqslant 0.15$, and oxygen content decreased with increasing Sr content for $x \geqslant 0.2$.

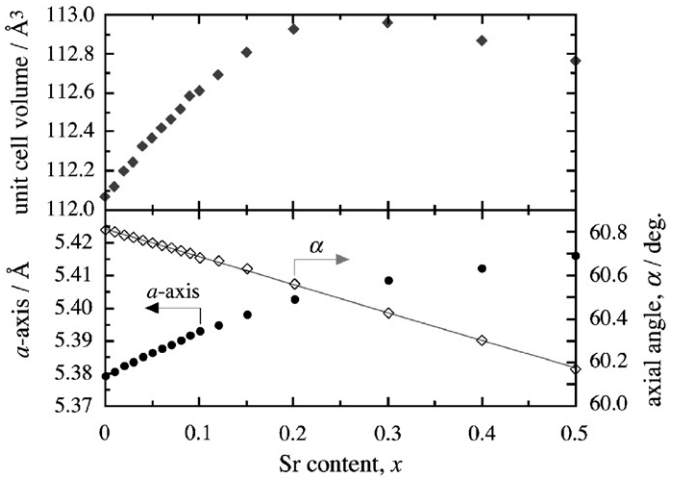

Fig. 1. Rhombohedral lattice parameters of $La_{1-x}Sr_xCoO_3$ at room temperature. The solid linear line is a guide for eyes. The standard deviations of the lattice parameters are lesser than plot size.

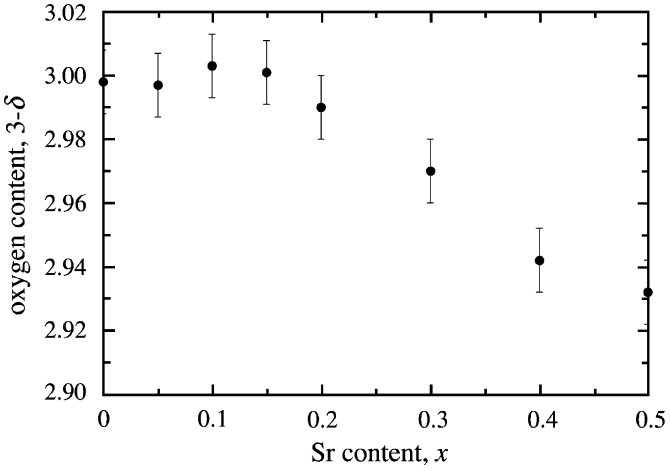

Fig. 2. Oxygen content in $La_{1-x}Sr_xCoO_{3-\delta}$.

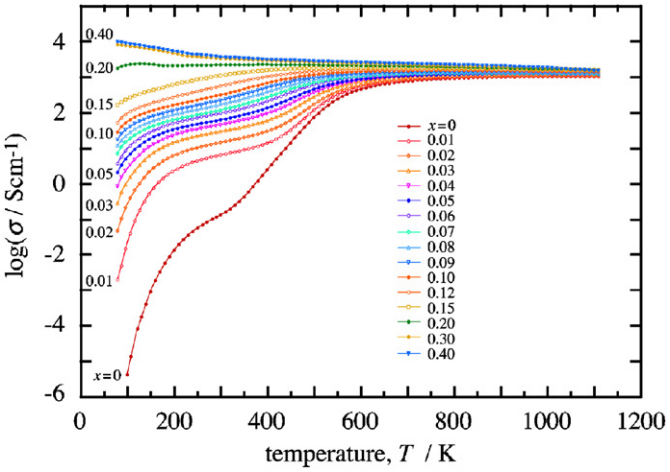

Fig. 3. (Color online) Temperature dependence of electrical conductivity of $La_{1-x}Sr_xCoO_3$. Solid lines are guide for eyes.

Fig. 3 shows the electrical conductivity (σ) of $La_{1-x}Sr_xCoO_3$ ($0 \leqslant x \leqslant 0.40$). At 300 K, σ (43 and 61 S cm^{-1} for $x = 0.04$ and 0.05, respectively) corresponds to that of single-crystal $La_{1-x}Sr_xCoO_3$ (33 S cm^{-1} to $x = 0.04$ [8] and 70 S cm^{-1} to $x = 0.05$ [11] at 300 K). It seems that the grain boundary does not significantly interrupt the carrier conduction for $La_{1-x}Sr_xCoO_3$. As shown in Fig. 3, σ increased with increasing Sr content, and the difference in σ among samples with different Sr content decreased with increasing temperature. For $0 \leqslant x \leqslant 0.20$, σ exhibited semiconducting behavior at lower temperatures, and showed a metal–insulator transition (MIT) at higher temperatures. MIT temperature decreased with increasing Sr content, e.g., 1050 K for $x = 0$ and 400 K for $x = 0.20$. For $x = 0.20$, a convex curve was also observed in the temperature range $100 \leqslant T \leqslant 200$ K as reported in previous studies [16,21,22]. For $0.30 \leqslant x \leqslant 0.40$, σ exhibited metallic behavior over the measured temperature range. On the whole, temperature and Sr-doping level dependencies of σ agrees well with previous studies [7,15–18,21,22,26–30]. For $x = 0.50$, there was a significant difference between σ measured from 300 to 1100 K (heating run) and from 1100 to 300 K (cooling run), and the difference was also observed in repeated measurements. Señarís-Rodríguez and Goodenough [16] in their thermogravimetric analysis have shown that the oxygen content in $La_{1-x}Sr_xCoO_{3-\delta}$ ($x > 0.25$) is different for heating and cooling runs above room temperature. Mineshige

et al. [26] have also reported that oxygen content depends on both heating (cooling) rate and temperature range for heavily Sr-doped samples. Thus, the difference in σ for $x = 0.50$ between the heating and the cooling runs is attributable to the difference in oxygen content. In the present study, such a difference was also shown for $x = 0.40$, although it was slight compared to that for $x = 0.50$.

The Hall coefficient was measured to evaluate carrier concentration (n) and the Hall mobility (μ) of $La_{1-x}Sr_xCoO_3$, and Fig. 4 shows n and μ. The Hall coefficient for $La_{0.99}Sr_{0.01}CoO_3$ (0.011 $cm^3\,C^{-1}$ at 300 K) corresponds to those of previous studies with the same composition, 0.009 $cm^3\,C^{-1}$ by Gerthsen and Härdtl [12] and 0.007 $cm^3\,C^{-1}$ by Tokura et al. [13]. As shown in Fig. 4, n increased with increasing Sr content for $0 \leqslant x \leqslant 0.15$, and slightly decreased for $0.20 \leqslant x \leqslant 0.40$. On the other hand, μ monotonically increased with Sr content. As a result, it was revealed that the increase in electrical conductivity resulted from increases in both n and μ for $0 \leqslant x \leqslant 0.15$, and from increase in μ for $0.20 \leqslant x \leqslant 0.40$.

In $La_{1-x}Sr_xCoO_3$, substitution of one Sr^{2+} yields one hole since the number of valence electrons of Sr is less by one than that of La. At 300 K, carrier concentration (n) is more than three times larger than Sr concentration for $0.01 \leqslant x \leqslant 0.15$. For example, n is $6.1 \times 10^{20}\,cm^{-3}$ for $x = 0.01$ and Sr concentration is 1.8×10^{20} cm^{-3}, suggesting that the doped carrier is already saturated at 300 K. For $0.20 \leqslant x \leqslant 0.40$, n decreases despite the increase in Sr content. This can be explained by increase in oxygen defects that is significantly formed for heavily Sr-doped samples as shown in Fig. 2, since oxygen defects counteract the hole produced by Sr-doping. Oxygen defect content (δ) estimated from carrier concentration, e.g., $\delta = 0.09(4)$ for $x = 0.40$ ($n = 5.9 \times 10^{21}\,cm^{-3}$), which is calculated assuming that n is $9.2 \times 10^{21}\,cm^{-3}$ for $La_{0.6}Sr_{0.4}CoO_3$ with no oxygen defect ($9.2 \times 10^{21}\,cm^{-3}$ is the maximum carrier concentration obtained in this study), approximately corresponds to $\delta = 0.06(1)$ that was determined by an iodometric titration (Fig. 2).

Fig. 5 shows the temperature dependencies of carrier concentration (n) and the Hall mobility (μ) for $La_{1-x}Sr_xCoO_3$ ($x = 0$ and 0.10). n of both samples increased with temperature, while no significant change in μ was observed. Thus, increase in electrical conductivity (σ) in temperature range $150 \leqslant T \leqslant 300$ K is mainly attributable to increase in n by thermal activation. Above 300 K, however, increase in σ is not explained by increase in n alone. For example, n at 1000 K (n_{1000}) is estimated to be $n_{1000} = n_{300}(\sigma_{1000}/\sigma_{300}) = 6.1 \times 10^{20}(1000/5.9) = 1.0 \times 10^{23}\,cm^{-3}$ (n_{300}, σ_{300}, and σ_{1000} are n at 300 K, σ at 300 K, and σ at 1000 K, respectively),

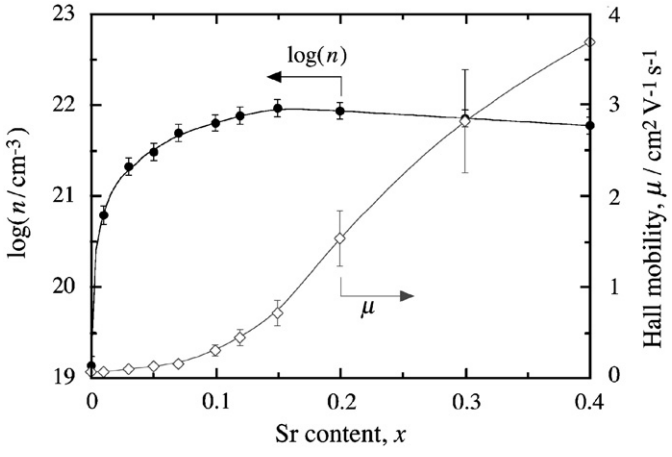

Fig. 4. Carrier concentration (n) and the Hall mobility (μ) of $La_{1-x}Sr_xCoO_3$ at 300 K. Solid lines are guide for eyes.

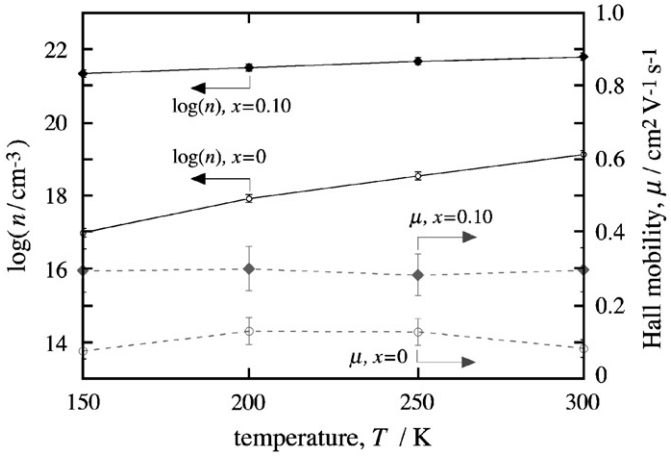

Fig. 5. Temperature dependence of carrier density (n) and the Hall mobility (μ) for $La_{1-x}Sr_xCoO_3$ ($x = 0$ and 0.10). Solid and dashed lines are guide for eyes.

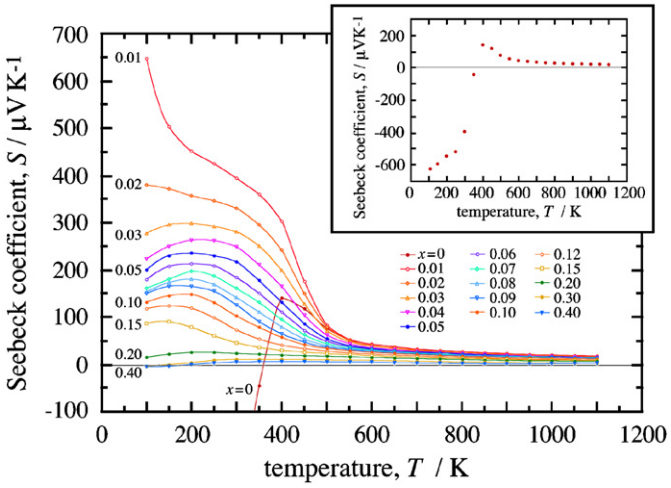

Fig. 6. (Color online) Temperature dependence of the Seebeck coefficient for $La_{1-x}Sr_xCoO_3$. The inset shows the Seebeck coefficient of non-doped $LaCoO_3$. Solid lines are guide for eyes.

assuming that increase in σ depends on only n. The estimated value ($1.0 \times 10^{23}\,cm^{-3}$) exceeds a carrier concentration of the order of $10^{22}\,cm^{-3}$ for metals. Thus, it can be deduced that not only n but also μ increase at higher temperatures.

Fig. 6 shows the Seebeck coefficient (S) of $La_{1-x}Sr_xCoO_3$ ($0 \leqslant x \leqslant 0.40$), and the inset shows S of non-doped $LaCoO_3$. As shown in the inset, S of $LaCoO_3$ was negative in the temperature range $100 \leqslant T \leqslant 350$ K, and the sign changed from negative to positive with increasing temperature. Then, S decreased with temperature above 400 K. The behavior is similar to that reported by Ohtani et al. [28] and Sehlin et al. [31]. On the other hand, several studies have reported a positive S at lower temperatures [1,15,25,32,33]. Moreover, Berggold et al. [8] have shown that both positive and negative S are observed for single-crystal $LaCoO_3$ even when grown under the same conditions. The differences in the sign of S are attributable to the formation of oxygen defects (or formation of Co^{2+}) [8,28,34,35], contamination of impurity elements [31], and/or deviation from the stoichiometric cation composition [36]. In contrast to the lower temperature range, each S shows similar value and temperature dependence above 500 K [15,25,28,31–33], indicating that S of $LaCoO_3$ is mainly

dominated by hole concentration, which is increased by thermal activation, at higher temperatures.

For Sr-doped samples, S decreased with increasing Sr content as shown in Fig. 6. The sign was positive for $0.01 \leqslant x \leqslant 0.20$ over the measured temperature range. As temperature increased, S decreased for $0.01 \leqslant x \leqslant 0.02$, while a maximum was observed around 200 K for $0.03 \leqslant x \leqslant 0.20$. For $0.30 \leqslant x \leqslant 0.40$, the sign of S changed from negative to positive with increasing temperature. The behavior of S agrees well with that reported by Berggold et al. [8] ($T < 300$ K). On the other hand, we could not obtain a large S ($\sim 700\,\mu V\,K^{-1}$ at $x = 0.05$ around 300 K) as reported by Androulakis et al. [1] and Kobayashi et al. [11]. In the present study, the highest S at 300 K is about $400\,\mu V\,K^{-1}$ for $x = 0.01$. This value is nonetheless much smaller than $700\,\mu V\,K^{-1}$.

The carrier effective mass (m^*) and the carrier relaxation time (τ) of $La_{1-x}Sr_xCoO_3$ ($0.01 \leqslant x \leqslant 0.40$) were estimated from the Seebeck coefficient (S) and carrier concentration (n) at 300 K using the following equations that are used for doped semiconductors [37–39]:

$$S = \frac{k_B}{e}\left(\frac{(s+5/2)F_{s+3/2}(\xi_F)}{(s+3/2)F_{s+1/2}(\xi_F)} - \xi_F\right), \quad (1)$$

$$F_s(\xi_F) = \int_0^\infty \frac{x^s}{1+e^{x-\xi_F}}\,dx, \quad (2)$$

$$n = 4\pi\left(\frac{2m^*k_BT}{h^2}\right)^{3/2} F_{1/2}(\xi_F), \quad (3)$$

$$\mu = \frac{e\tau}{m^*}, \quad (4)$$

where k_B is the Boltzmann constant, e the elementary electric charge, s the scattering parameter, F_s the Fermi integral (Eq. (2)), ξ_F the reduced chemical potential, and h the Planck constant. Ionized impurity scattering ($s = 3/2$) was assumed to be dominant in the calculation. When other scattering mechanisms were adopted, the Sr-doping level dependencies of m^* and τ were qualitatively similar to each other, although the magnitudes of m^* and τ depended on the scattering parameter, e.g., $m^* = 51m_e$ (m_e is the rest mass of electrons) for $x = 0.01$ when acoustic phonon scattering ($s = -1/2$) was assumed to be dominant. As shown in Fig. 7, m^* decreased with increasing Sr content, and τ increased for $0.01 \leqslant x \leqslant 0.20$ and decreased for $0.20 \leqslant x \leqslant 0.40$. These results explain that the increase in mobility (μ) by Sr-doping (Fig. 4) is caused by both decrease in m^* and increase in τ for $0.01 \leqslant x \leqslant 0.20$, and by decrease in m^* for $0.20 \leqslant x \leqslant 0.40$. In addition, it was revealed that the decrease in the Seebeck coefficient (S) by Sr-doping (Fig. 6) resulted from the decrease in m^* as well as the increase in n (Fig. 4).

In perovskite-type AMO_3 ($M = 3d$ transition metals), $M3d$–$O2p$ hybridization affects the electrical properties since $M3d$–$O2p$ hybridization mainly determines the electronic structure around the Fermi level. For example, in $RNiO_3$ (R = rare earth), an increase in Ni–O–Ni bond angles increases the bandwidth around the Fermi level [40], leading to a transition from insulating to metallic. In $La_{1-x}Sr_xCoO_3$, Sr-doping relaxes the rhombohedral distortion of the $LaCoO_3$ lattice and increases Co–O–Co bond angles between adjacent CoO_6 octahedra [19,26]. Thus, the bandwidth increases with increasing Sr content, and as a result, the carrier effective mass (m^*) decreases. In addition, when temperature increases, the Co–O–Co bond angles also increase [19,26,41], and hence it can be inferred that m^* also decreases with temperature and mobility (μ) increases at higher temperatures as discussed above. These considerations suggest that Sr-doping and a temperature increase have similar effects on transport properties of $La_{1-x}Sr_xCoO_3$.

In contrast to the decrease in m^*, carrier relaxation time (τ) increased for $0.01 \leqslant x \leqslant 0.20$ (Fig. 7). This is also attributable to the increase in Co–O–Co bond angles [19,26] and the relaxation of rhombohedral distortion by Sr-doping. The decrease in τ for $0.20 \leqslant x \leqslant 0.40$ may be due to enhancement of point-defect scattering caused by formation of oxygen defects that is significant for heavily Sr-doped samples.

Fig. 8 shows power factor (σS^2) of $La_{1-x}Sr_xCoO_3$: (a) σS^2 vs. temperature and (b) σS^2 vs. Sr content. For Sr-doped samples, a maximum was observed in the temperature range $100 \leqslant T \leqslant 400$ K (Fig. 8(a)). As shown in Fig. 8(b), σS^2 showed its maximum at around $x = 0.10$, and decreased with increasing Sr content. Decreases in σS^2 at higher temperatures and/or for heavily Sr-doped samples are mainly due to the decrease in the Seebeck coefficient as shown in Fig. 6. The highest σS^2 was 3.7×10^{-4} W m^{-1} K^{-2} for $x = 0.10$ at 250 K. However, the value is lesser than the 18×10^{-4} W m^{-1} K^{-2} reported by Androulakis et al. [1] ($x = 0.05$ at 300 K) because of the large difference in the Seebeck coefficient.

Thermal conductivity of $La_{1-x}Sr_xCoO_3$ at 300 K normalized to 95% of theoretical density is shown in Fig. 9. The following

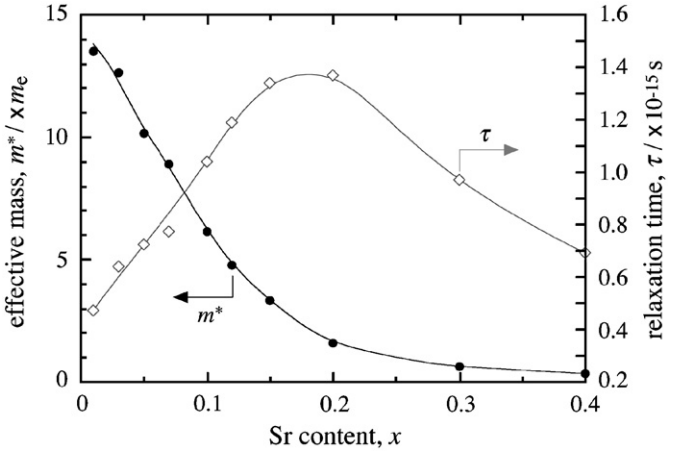

Fig. 7. Carrier effective mass (m^*) and relaxation time (τ) of $La_{1-x}Sr_xCoO_3$ ($0.01 \leqslant x \leqslant 0.40$) at 300 K. Solid lines are guide for eyes.

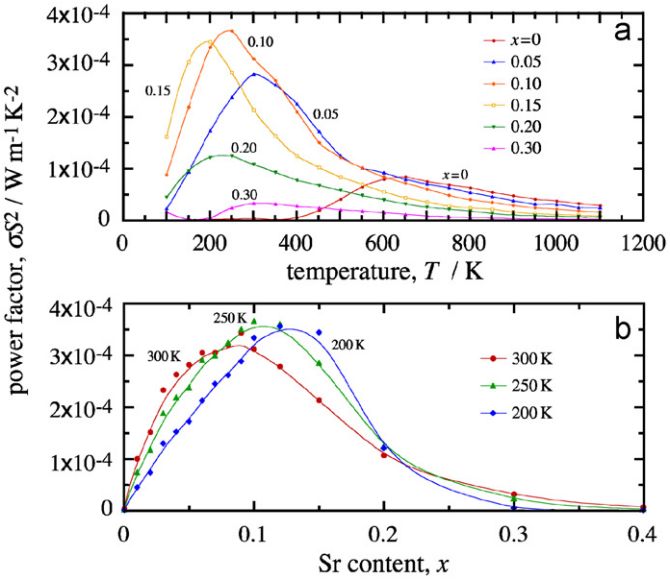

Fig. 8. (Color online) Power factor of $La_{1-x}Sr_xCoO_3$: (a) power factor vs. temperature and (b) power factor vs. Sr content. Solid lines are guide for eyes.

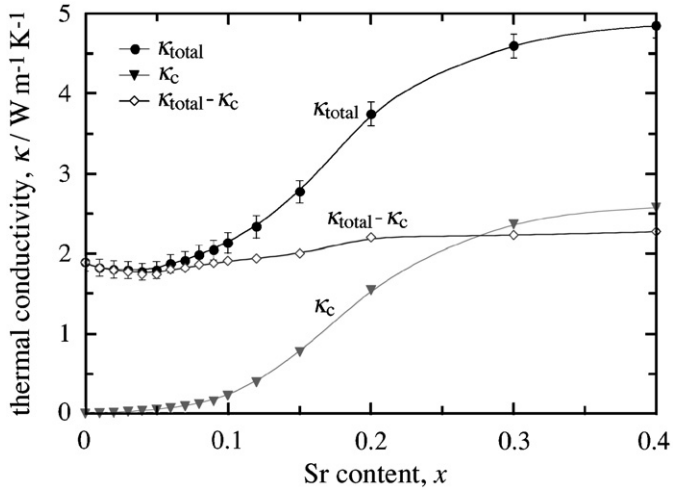

Fig. 9. Thermal conductivity of $La_{1-x}Sr_xCoO_3$ at 300 K. κ_{total} is the normalized value to 95% of theoretical density and κ_c is the thermal conductivity by charged carrier. Solid lines are guide for eyes.

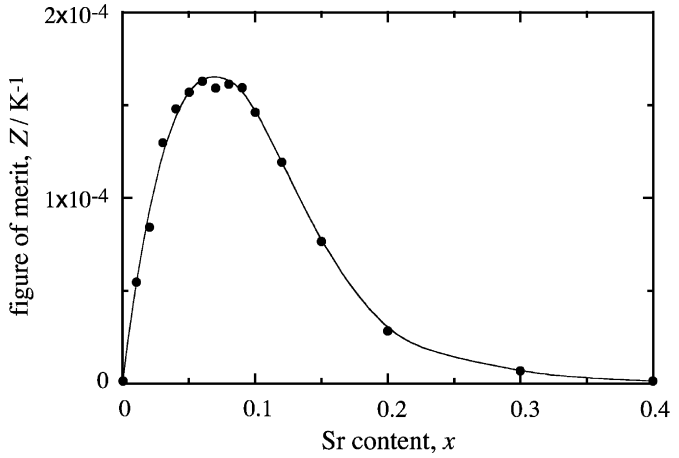

Fig. 10. Figure of merit of $La_{1-x}Sr_xCoO_3$ at 300 K. The solid line is a guide for eyes.

equation was used for density correction [42]:

$$\kappa_{total} = \kappa \frac{(0.95)^{1.5}}{(1-P)^{1.5}}, \quad (5)$$

where κ_{total} is normalized thermal conductivity, κ the measured thermal conductivity, and P the fractional porosity of the pellet. As shown in Fig. 9, κ_{total} decreased for $0 \leqslant x \leqslant 0.04$ and increased for $x \geqslant 0.05$ with increasing Sr content. The increase for $x \geqslant 0.05$ is mainly due to the heat transport by the conductive carrier (κ_c) as plotted in Fig. 9 using the Wiedemann–Franz law ($\kappa_c = \sigma LT$; L is the Lorenz number $= 2.45 \times 10^{-8}\,V^2\,K^{-2}$). The heat transport by phonon is included in the difference between κ_{total} and κ_c ($\kappa_{total} - \kappa_c$), and is generally reduced by doping of other elements because of enhancement of phonon-point-defect scattering. However, the Sr-doping level dependence of $\kappa_{total} - \kappa_c$ was slight as reported for single-crystal $La_{1-x}Sr_xCoO_3$ [8]. $\kappa_{total} - \kappa_c$ (about $2\,W\,m^{-1}\,K^{-1}$) was about 60–70% of that for $La_{1-x}Sr_xCoO_3$ crystals (about $3\,W\,m^{-1}\,K^{-1}$) [8], probably because of phonon scattering at grain boundary in polycrystalline samples.

Fig. 10 shows the figure of merit ($Z = \sigma S^2 \kappa^{-1}$) of $La_{1-x}Sr_xCoO_3$ at 300 K. Z was maximum at around $x = 0.06$ and rapidly decreased for $x \geqslant 0.10$. Decrease in Z for heavily Sr-doped samples is attributed to both the decrease in the Seebeck coefficient (S) and increase in thermal conductivity (κ). The highest Z at 300 K is $1.6 \times 10^{-4}\,K^{-1}$ for $x = 0.06$ ($ZT = 0.048$), which is comparable to that for a $La_{1-x}Sr_xCoO_3$ crystal ($Z = 1.5 \times 10^{-4}\,K^{-1}$ for $x = 0.125$ at 225 K ($ZT = 0.035$)) [8]. On the other hand, the value is lesser than the $6.0 \times 10^{-4}\,K^{-1}$ ($x = 0.05$ at 300 K, $ZT = 0.18$) reported by Androulakis et al. [1] because of the difference in the Seebeck coefficient (S) as mentioned above. At higher temperatures, thermoelectric properties of $La_{1-x}Sr_xCoO_3$ would be diminished since power factor (σS^2) decreases with temperature as shown in Fig. 8. In addition, a remarkable reduction in κ is not also expected because of the increase in heat transport by the conductive carrier at higher temperatures, e.g., κ_c is calculated to be $2.4\,W\,m^{-1}\,K^{-1}$ for $LaCoO_3$ at 1000 K. In fact, Zhang et al. [9] has reported that Z of $La_{0.95}Sr_{0.05}CoO_3$ decreases with increasing temperature in the temperature range $300 \leqslant T \leqslant 750$ K.

4. Conclusions

The thermoelectric properties of perovskite-type $La_{1-x}Sr_xCoO_3$ have been investigated. The substitution of Sr^{2+} leads to increases in carrier concentration (n) and the Hall mobility (μ), and a decrease in carrier effective mass (m^*), resulting in an increase in electrical conductivity (σ) and a decrease in the Seebeck coefficient (S). The decrease in m^* can be explained by an increase in bandwidth caused by an increase in Co–O–Co bond angles. The results of σ, S, and the Hall coefficient measurements also suggest that temperature increase and Sr-doping have similar effects on electrical properties of $La_{1-x}Sr_xCoO_3$. Thermoelectric properties of $La_{1-x}Sr_xCoO_3$ are improved by Sr-doping, although heavy Sr-doping decreases the performances due to decrease in S and increase in thermal conductivity (κ). The figure of merit of $La_{1-x}Sr_xCoO_3$ is still low compared to those of layered cobalt oxides such as Na_xCoO_2. However, thermoelectric properties would be enhanced by realizing a high S as shown by Androulakis et al. [1] and Kobayashi et al. [11]. Further investigations are necessary for understanding the large differences in S among the samples of similar chemical compositions.

Acknowledgments

This work was partly supported by The Thermal & Electric Energy Technology Foundation. The Hall coefficient measurement was performed using the facility of the Akasaki Research Center in Nagoya University. The authors wish to express their gratitude to Dr. Masahito Yamaguchi and Dr. Yoshio Honda in Nagoya University, and Dr. Shingo Ohta in Toyota Central R&D Labs., Inc. for their cooperation in measuring the Hall coefficient.

References

[1] J. Androulakis, P. Migiakis, J. Giapintzakis, Appl. Phys. Lett. 84 (2004) 1099–1101.
[2] T. Okuda, K. Nakanishi, S. Miyasaka, Y. Tokura, Phys. Rev. B 63 (2001) 113104.
[3] H. Muta, K. Kurosaki, S. Yamanaka, J. Alloys Compd. 368 (2004) 22–24.
[4] S. Ohta, T. Nomura, H. Ohta, K. Koumoto, J. Appl. Phys. 97 (2005) 034106.
[5] T. Kobayashi, H. Takizawa, T. Endo, T. Sato, M. Shimada, H. Taguchi, M. Nagao, J. Solid State Chem. 92 (1991) 116–129.
[6] M. Ohtaki, H. Koga, T. Tokunaga, K. Eguchi, H. Arai, J. Solid State Chem. 120 (1995) 105–111.
[7] T. Takami, H. Ikuta, U. Mizutani, Trans. Mater. Res. Soc. Japan 29 (2004) 2777–2780.
[8] K. Berggold, M. Kriener, C. Zobel, A. Reichl, M. Reuther, R. Müller, A. Freimuth, T. Lorenz, Phys. Rev. B 72 (2005) 155116.
[9] X. Zhang, X.M. Li, T.L. Chen, L.D. Chen, J. Cryst. Growth 286 (2006) 1–5.
[10] T.H.J. Chen, T.G. Calvarese, M.A. Subramanian, Solid State Sci. 8 (2006) 467–469.
[11] Y. Kobayashi, S. Murata, K. Asai, J.M. Tranquada, G. Shirane, K. Kohn, J. Phys. Soc. Japan 68 (1999) 1011–1017.
[12] V.P. Gerthsen, K.H. Härdtl, Z. Naturforsch. 17a (1962) 514–521.

[13] Y. Tokura, Y. Okimoto, S. Yamaguchi, H. Taniguchi, T. Kimura, H. Takagi, Phys. Rev. B 58 (1998) R1699–R1702.
[14] P.M. Raccah, J.B. Goodenough, J. Appl. Phys. 39 (1968) 1209–1210.
[15] V.G. Bhide, D.S. Rajoria, C.N.R. Rao, G.R. Rao, V.G. Jadhao, Phys. Rev. B 12 (1975) 2832–2843.
[16] M.A. Señarís-Rodríguez, J.B. Goodenough, J. Solid State Chem. 118 (1995) 323–336.
[17] S. Yamaguchi, H. Taniguchi, H. Takagi, T. Arima, Y. Tokura, J. Phys. Soc. Japan 64 (1995) 1885–1888.
[18] R. Mahendiran, A.K. Raychaudhuri, Phys. Rev. B 54 (1996) 16044–16052.
[19] R. Caciuffo, D. Rinaldi, G. Barucca, J. Mira, J. Rivas, M.A. Señarís-Rodríguez, P.G. Radaelli, D. Fiorani, J.B. Goodenough, Phys. Rev. B 59 (1999) 1068–1078.
[20] K. Muta, Y. Kobayashi, K. Asai, J. Phys. Soc. Japan 71 (2002) 2784–2791.
[21] M. Kriener, C. Zobel, A. Reichl, J. Baier, M. Cwik, K. Berggold, H. Kierspel, O. Zabara, A. Freimuth, T. Lorenz, Phys. Rev. B 69 (2004) 094417.
[22] Y. Onose, Y. Tokura, Phys. Rev. B 73 (2006) 174421.
[23] F. Izumi, T. Ikeda, Mater. Sci. Forum 198 (2000) 321–323.
[24] J. Mizusaki, Y. Mima, S. Yamauchi, K. Fueki, H. Tagawa, J. Solid State Chem. 80 (1989) 102–111.
[25] J. Mizusaki, J. Tabuchi, T. Matsuura, S. Yamauchi, K. Fueki, J. Electrochem. Soc. 136 (1989) 2082–2088.
[26] A. Mineshige, M. Kobune, S. Fujii, Z. Ogumi, M. Inaba, T. Yao, K. Kikuchi, J. Solid State Chem. 142 (1999) 374–381.
[27] A. Mineshige, M. Inaba, T. Yao, Z. Ogumi, K. Kikuchi, M. Kawase, J. Solid State Chem. 121 (1996) 423–429.
[28] T. Ohtani, K. Kuroda, K. Matsugami, D. Katoh, J. Eur. Ceram. Soc. 20 (2000) 2721–2726.
[29] H. Masuda, T. Fujita, T. Miyashita, M. Soda, Y. Yasui, Y. Kobayashi, M. Sato, J. Phys. Soc. Japan 72 (2003) 873–878.
[30] Y. Kashiwada, H. Fujishiro, Y. Fujine, M. Ikebe, J. Hejtmanek, Physica B 378–380 (2006) 529–531.
[31] S.R. Sehlin, H.U. Anderson, D.M. Sparlin, Phys. Rev. B 52 (1995) 11681.
[32] G.H. Jonker, Philips Res. Rep. 24 (1969) 1–14.
[33] R.R. Heikes, R.C. Miller, R. Mazelsky, Physica 30 (1964) 1600–1608.
[34] S. Hébert, D. Flahaut, C. Martin, S. Lemonnier, J. Noudem, C. Goupil, A. Maignan, J. Hejtmanek, Prog. Solid State Chem. 35 (2007) 457–467.
[35] R. Robert, L. Bocher, M. Trottmann, A. Reller, A. Weidenkaff, J. Solid State Chem. 179 (2006) 3893–3899.
[36] J. Mizusaki, T. Sasamoto, W.R. Cannon, H.K. Bowen, J. Am. Ceram. Soc. 65 (1982) 363–368.
[37] S. Ohta, T. Nomura, H. Ohta, K. Koumoto, J. Appl. Phys. 97 (2005) 034106.
[38] R. Sakata, Netsuden Henkan Kogaku (Thermoelectrics), Realize, Tokyo, 2001, pp. 39–112 (in Japanese).
[39] R. Sakata, Netsuden Henkan (Thermoelectric Energy Conversion), Shokabo, Tokyo, 2005, pp. 10–83 (in Japanese).
[40] J.B. Torrance, P. Lacorre, A.I. Nazzal, E.J. Ansaldo, Ch. Niedermayer, Phys. Rev. B 45 (1992) 8209–8212.
[41] P.M. Raccah, J.B. Goodenough, Phys. Rev. 155 (1967) 932–943.
[42] B. Schulz, High Temp. High Press. 13 (1981) 649–660.